Carbohydrate Polymers 111 (2014) 492–504

Contents lists available at ScienceDirect

Carbohydrate Polymers

journal homepage: www.elsevier.com/locate/carbpol

# Amorphous supramolecular structure of carboxymethyl cellulose in aqueous solution at different pH values as determined by rheology, small angle X-ray and light scattering

Iztok Dogsa[a], Matija Tomšič[b], Janez Orehek[c], Elizabeta Benigar[b], Andrej Jamnik[b], David Stopar[a,*]

[a] Biotechnical Faculty of Ljubljana University, Chair of Microbiology, Večna pot 111, 1000 Ljubljana, Slovenia
[b] Faculty of Chemistry and Chemical Technology, University of Ljubljana, Chair of Physical Chemistry, Aškerčeva 5, 1000 Ljubljana, Slovenia
[c] JUB-H d. d., Dol pri Ljubljani 28, 1262 Dol pri Ljubljani, Slovenia

ARTICLE INFO

*Article history:*
Received 23 September 2013
Received in revised form 14 March 2014
Accepted 7 April 2014
Available online 22 April 2014

*Keywords:*
CMC
SAXS
DLS
String-of-beads model
Carboxymethyl Cellulose
Macromolecular structure
Supramolecular structure

ABSTRACT

Carboxymethyl cellulose (CMC) is one of the most widely used thickening agents in industry. The combination of small-angle X-ray scattering (SAXS), static and dynamic light scattering, as well as viscosity measurements and microscopy at different pH values was utilized to explore the physicochemical properties of CMC on a scale ranging from individual macromolecules to supramolecular assemblies. The supramolecular structure of CMC was represented as a set of characteristic sample subspaces based on SAXS data utilizing the string-of-beads model. The results indicate that at pH 7.0 individual CMC molecules are approximately uniformly distributed in a supramolecular structure owing to strong intra- and intermolecular repulsive interactions. The structure of CMC is most expanded at the value of $pK_a$, where it has the largest radius of gyration, persistence length, and size of heterogeneous regions. Below $pK_a$ the majority of the CMC sample volume belongs to the low density subspaces. Most of CMC molecules, however, reside in a few high density subspaces. Dynamically, supramolecular structure of CMC is composed of fast diffusive relaxation processes embedded in a background of non-diffusive slow relaxation process at high pH and mostly slow relaxation processes at low pH. The rheological properties of CMC at different pH values were directly related to the CMC supramolecular structure in the aqueous environment.



## 1. Introduction

The term supramolecular structure refers to the structural organization of molecules, i.e. the structure beyond the individual molecule. One way to obtain detailed insight into the supramolecular structure of carbohydrate polymer systems is to model each individual polymer molecule as an assembly of monomers held together by covalent bonds, and to numerically simulate a system with a number of such polymer molecules involving intermolecular interactions. For polysaccharides where local molecular order is expected to be intermediate between the randomly coiled chain and the rigid helix, simple models do not give an acceptable result. To remedy this, a more complex modelling of broken rod-like chains may be applied. In such models individual segments (i.e. coils or helices) are linked together in a random orientation assuming equal averaged lengths, which is an obvious simplification. To improve modelling realism further the length of the rod-like chain segment should be shortened ultimately to the size of an individual monomer. In this work monomers were modelled as spheres with the dimensions of anhydroglucose unit (i.e. 5.2 Å). Individual spheres were connected to a string of beads. We have demonstrated in our previous work a good correspondence between the string of beads model and the atomistic model of short oligomer polysaccharides (Dogsa, Štrancar, Laggner, & Stopar, 2008). Such an approach implies that the ideas, which have been very successful in describing the structure of individual polymer molecules, may also be successful in describing supramolecular structures of carbohydrates (Turro, 2005). It has been suggested that cellulose derivatives (e.g. cellulose trinitrate) can form supramolecular structures in solution (Schurz, 1983). To the best of our knowledge, there has

* Corresponding author at: Chair of Microbiology, Department of Food Science and Technology Biotechnical Faculty, University of Ljubljana, Večna pot 111, 1000 Ljubljana, Slovenia. Tel.: +386 1 320 3412; fax: +386 1 257 33 90.
*E-mail address:* david.stopar@bf.uni-lj.si (D. Stopar).

http://dx.doi.org/10.1016/j.carbpol.2014.04.020
0144-8617/

so far been no detailed study of the supramolecular structure of carboxymethyl cellulose (CMC) in aqueous solutions at different pH values.

CMC is a modified water soluble cellulose with unparalleled applicability in different branches of industry (e.g. food processing, pharmaceuticals, adhesives, paints, leather, paper, textiles, ceramics, agricultural products, detergents, as well in oil well drilling, foundry work and mineral processing). In industrial applications CMC is primarily used for controlling product viscosity and at the same time avoiding gelling. It therefore acts as a thickener, phase and emulsion stabilizer, and/or suspension agent. CMC is biocompatible and it was recently shown that it can be used to form pectin/carboxymethyl cellulose/microfibrillated cellulose composite scaffolds for tissue engineering (Ninan et al., 2013). CMC has a large water-holding capacity, which is high even in samples with low viscosities (Cummings & Stephen, 1979). It is an anionic linear polyelectrolyte and its molecular conformation in aqueous solution strongly depends on the concentration, ionic strength and pH value (Wandrey, Bartowiak, & Harding, 2009). Above the overlap concentration thermo-reversible hydrogels are formed in aqueous systems, as for example in carrageenan (Yuguchi, 2009). The critical overlap concentration of polymer coils, denoted $c^*$, is one of the most important characteristic values of a polymer solution. It is generally accepted that at concentrations $c/c^* < 1$ the steric and frictional interactions of neighbouring polymer coils are negligible and the rheological response of the fluid is solely governed by the sum of the deformation and hydrodynamic interactions of the isolated polymer coils and solvent which comprise the polymer solution. When these conditions exist, the theoretical description of a dilute solution given by the Rouse/Zimm theory is expected to be valid. At higher concentrations the solution becomes semi-dilute and polymers get eventually entangled depending on the degree of overlap of adjacent coils and their molar mass (Clasen et al., 2006). With heavy metals, three-valent cations and the majority of polycations CMC may form complexes (Wandrey et al., 2009). The average chain length of the cellulose backbone and the average degree of substitution (in terms of carboxymethyl units) strongly influence the properties of each individual CMC type; the more-hydrophobic lower substituted CMCs are thixotropic, but the more-extended higher substituted CMCs are pseudoplastic. At low pH, CMC may cross-link through lactonization between carboxylic acid and free hydroxyl groups (Emeje, Kunle, & Ofoefule, 2006). It is fairly stable over a pH range of 5.0–10.0, but acidification below a pH value of 5.0 reduces its viscosity and its long term stability. The polymer chains of CMC are most extended at low concentrations, low ionic strengths, and high values of pH (Kästner, Hoffmann, Dönges, & Hilbig, 1997). Despite CMC's immense importance the methods for its physico-chemical descriptions are still evolving (Shakun, Maier, Heinze, Kilz, & Radke, 2013; Shakun, Heinze, & Radke, 2013).

It is extremely difficult to investigate the supramolecular structure of CMC in detail, as it spans different length- and time-scales. High-resolution techniques of crystallography and NMR are not applicable in the case of CMC due to the lack of a regular lattice in the structure and high molecular mass, respectively. There have been several attempts reported in the literature to characterize the macroscopic properties of CMC by its microscopic structure (Adel, Abou-Youssef, El-Gendy, & Nada, 2010; Benchabane & Bekkour, 2008; Kästner et al., 1997; Kulicke et al., 1996). Most notably, the thickening properties of a polymer solution are related to the rigidity of the backbone, which is in turn characterized by the polymer persistence length. The persistence length of the polymer backbone can be obtained from intrinsic viscosity measurements (Yamakawa & Fujii, 1974). Light and X-ray scattering techniques, on the other hand, are well-suited to characterize molecular weight distribution, conformation or supramolecular structure of polymers in solution (Berne & Pecora, 2000; Brown & Mortensen, 2000; Sharma & Bohidar, 2000), including carbohydrate polymers (Dogsa et al., 2008; Doutch & Gilbert, 2013; Doutch et al., 2012; Josef & Bianco-Peled, 2012; Orehek et al., 2013; Roblin et al., 2013; Wang, Blazek, Gilbert, & Copeland, 2012). Small-angle neutron scattering has revealed that CMC behaves as a Gaussian distribution of rigid segments and that its persistence length increases with dilution and charge density (Moan & Wolff, 1975). In addition, the small-angle X-ray scattering (SAXS) technique offers the possibility of analysing polymer sample in terms of the distribution of molecular dimensions, represented by the radius of gyration, the repulsion interaction correlation length, the persistence length and the size of heterogeneous regions. The persistence length of CMC in aqueous solutions estimated by SAXS was in the range of 2–4 nm (Muroga, Yamada, Noda, & Nagasawa, 1987). In another study the persistence length determined by Size Exclusion Chromatography – Multi-Angle Laser Light Scattering (SEC-MALLS) and potentiometric titration was estimated to be around 5.6 nm, whereas electrostatic persistence length was 1.6 nm at low salt and 0.3 nm at high salt concentration (Hoogendam et al., 1998). When complexed with alkaline earth metal ions, the radius of gyration of CMC as determined by SAXS significantly increased (Matsumoto & Zenkoh, 1992). Recent developments in the data analysis of SAXS experiments (Dogsa, Kriechbaum, Stopar, & Laggner, 2005; Dogsa et al., 2008; Orehek et al., 2013), which enable one to obtain the structural and interaction parameters of polymers, provide a very promising new tool for probing the supramolecular organization of carbohydrate polymers in solution and were further explored and developed in this work.

In this study carboxymethyl cellulose with a molecular mass of 90 kDa and a 0.7 degree of substitution was used. Samples prepared at different pH values were investigated by SAXS, static and dynamic light scattering (SLS, DLS) and viscosimetry. As CMC is a polyelectrolyte, the repulsion between charged segments, the radius of gyration, repulsion interaction correlation length, persistence length, and the size of heterogeneous regions were modelled. The string-of-beads model (Dogsa et al., 2008; Orehek et al., 2013) was improved to account for Debye–Bueche inhomogeneities and was used to analyse CMC SAXS data. In the second step a new approach to estimate and visualize the macromolecular structure of CMC was developed. For this purpose various molecular shape parameters representing single helices with different pitch values, number of monomers per pitch, cross-sectional radius and different random coil content were used to describe the secondary structure elements of CMC. The distribution of local volume fraction of CMC polymers in supramolecular structure was calculated on the basis of the results obtained from SAXS data. The CMC supramolecular structure was represented graphically as a collection of subspaces at different pH values. The combined rheological, SLS, DLS and SAXS parameters were used to discuss structural and dynamic behaviour of CMC supramolecular structure. We believe that the improved approach could be of broader physico-chemical interest in polymer and particular carbohydrate polymer community.

## 2. Experimental and theoretical methods

### 2.1. Materials and sample preparation

The sodium salt of CMC (NaCMC) was purchased from Sigma–Aldrich ($M_w$(NaCMC) = 90 kDa; $M_w$ (dissociated form) = 82 kDa; degree of substitution DS = 0.7). Molecular mass of the polymer was verified by static light scattering (SLS) via the construction of the well-known Zimm-plot (Zimm, 1948). For this purpose the densities $\rho$ of aqueous CMC solutions were carefully measured at 25 °C utilizing the Anton Paar density meter DMA 5000. The refractive index increment $dn/dc$ of 0.141 mL g$^{-1}$ was

determined for CMC in water based on the measurements with the differential refractometer DnDc-2010 WGE DR. BURES. The two extrapolations in the Zimm plot (Appendix A) to zero polymer concentration and zero scattering angle resulted in Mass average molecular mass $M_w$ of $81 \pm 7$ kDa, which is in good agreement with the value specified from the manufacturer and by our size exclusion chromatography (HPSEC) (Orehek et al., 2013).

Samples for SAXS, DLS, SLS and viscosity measurements were prepared as 2% (w/v) CMC in 0.1 M electrolyte solutions. This concentration was chosen because it offered sufficient scattering power for SAXS experiments. To keep the ionic strength constant at different pH values, a 3% CMC stock solution and 0.3 M aqueous solutions of HCl and NaCl were prepared in distilled water and mixed in appropriate ratios. To obtain the desired value of pH, 3% CMC was mixed with different mixtures of HCl/NaCl in a volume ratio of 2:1. Mixtures of HCl/NaCl in volume ratios 1:0, 1:1, 7:13, 1:19, 0:1 were used to obtain pH values of 1.6, 3.1, 3.6, 5.0, and 7.0, respectively. For the intrinsic viscosity measurements, the CMC concentration series was prepared by diluting 2% CMC samples with distilled water and electrolyte mixture (2:1). The appropriate pH values were adjusted by addition of concentrated NaOH.

### 2.2. Small-angle X-ray scattering measurements

Small-Angle X-Ray Scattering (SAXS) spectra were measured at 25 °C with a Kratky compact camera (Anton Paar KG, Graz, Austria) (Kratky & Stabinger, 1984), which was modified to enclose the focusing multilayer optics for the primary X-ray beam (Göbel mirror; Osmic). The camera was attached to a conventional Kristalloflex 760 X-ray generator (Bruker AXS GmbH, Karlsruhe, Germany) equipped with a sealed X-ray tube (Cu $K_\alpha$ X-rays with a wavelength $\lambda = 0.154$ nm) and operating at 40 kV and 35 mA. Focusing multilayer optics and a block-collimating unit provided an intense monochromatic primary beam that was attenuated by a Ni foil of appropriate thickness due to the limitations of the detector. In addition, a software monochromator was used to register only the scattered X-ray photons within a predefined range of energies. The samples were measured in a standard quartz capillary with an outer diameter of 1 mm and wall thickness of 10 μm. The scattered X-ray intensities were detected with a PSD-50 M ASA position sensitive detector (M. Braun GmbH, Garching, Germany) in the small-angle regime of scattering vectors given by $0.07 < q < 7\ \mathrm{nm}^{-1}$, where $q = 4\pi/\lambda \cdot \sin(2\vartheta)$ and $2\vartheta$ represents the scattering angle. Each individual sample was measured for at least 48 h to yield reliable measurement statistics. Each hour partial measurements were recorded to check for potential sample instability. Prior to further analysis the scattering data were corrected for the empty capillary and pure solvent scattering, and put to an absolute scale using water as a secondary standard (Orthaber, Bergmann, & Glatter, 2000).

### 2.3. Static and dynamic light scattering measurements

For SLS and DLS measurements we used a 3D-DLS Spectrometer (LS Instruments, Switzerland), equipped with a 35 mW He–Ne laser ($\lambda = 632.8$ nm), high precision beam-splitter, focusing entrance and collimating exit lens and two single-mode fibre-optic detectors with avalanche photodiodes (photo detection efficiency > 65%). Samples in scattering cells were immersed in a large-diameter thermostated bath (25 °C) of index matching liquid (decalin). Utilizing the primary-beam attenuator, the counting rates were adjusted to about 500 kHz. The instrument was used in a 3D-cross-correlation scheme. DLS measurements of 30 s each were collected and at least 15 of them were averaged to obtain the final autocorrelation function. The SLS intensities were obtained simultaneously during the DLS measurements. These measurements were performed at various scattering angles from 80° to 140° with a step of 10°. Prior to measurements the samples were centrifuged for 5 min at approximately $2500 \times g$, transferred to the measuring cell, left overnight and then carefully transferred (without shaking) to the measuring position in the goniometer – as checked by the density measurements such centrifugation had no detectable effect on the sample concentrations.

### 2.4. Viscosity measurements

Viscosity was measured on an Anton Paar Physica MCR 301 rotational rheometer. We used the plate-plate system with a plate diameter of 49.98 mm. The distance between plates was 0.25 mm and the measuring temperature was $(25.00 \pm 0.01)$ °C. Approximately 490 μL of sample was applied to fill the gap between the plates. Flow curves in a shear rate ranging from 10 to 1000 $s^{-1}$ were measured in 20 constant logarithmically-spaced steps with a time delay of 5 s between successive measurements. The results for viscosity measurements are reported at a shear rate of 1000 $s^{-1}$. The intrinsic viscosities were determined by measuring the viscosity of diluted samples. The intrinsic viscosity was determined by graphically evaluating the limit of the following equation:

$$[\eta] = \lim_{\gamma \to 0} \frac{\eta - \eta_0}{\eta_0 \gamma} \tag{1}$$

where $[\eta]$ is the intrinsic viscosity, $\eta$ viscosity of diluted polymer solution, $\eta_0$ viscosity of pure solvent, and $\gamma$ mass concentration of solute in $\mathrm{g/cm}^3$.

### 2.5. Evaluation of SAXS data

#### 2.5.1. Theoretical calculations of SAXS intensities and modelling

In the present study we modelled the scattering contributions of individual polymer chains by our string-of-beads model that we have already successfully applied on different polysaccharide systems including CMC (Dogsa et al., 2008; Orehek et al., 2013), where the scattering contributions due to interactions among individual chains were described by repulsion Gaussian interaction (Coviello et al., 1998; Dogsa et al., 2008; Likos et al., 2001, 2002; Orehek et al., 2013; Yuguchi, Urakawa, & Kajiwara, 2002). For such system the scattering function can be written in a form:

$$I(q) = \frac{\Delta\rho^2 \langle \varphi \rangle v_0}{1 + K e^{-q^2\xi^2}} \bar{p(q)} \tag{2}$$

where $v_0$ is the single polymer chain volume, $\langle \varphi \rangle$ is the mean volume fraction of the polymer, $K$ is the constant proportional to the strength of the repulsive interactions, $\xi$ is the correlation length over which the repulsion occurs, $\Delta\rho^2$ is the scattering length density difference between polymer and solvent, and $\bar{p(q)}$ is the representative chain form factor that we have calculated by the string of beads model (Dogsa et al., 2008; Orehek et al., 2013). Briefly, in this model the polymer is simulated with a linear chain of $N$ beads with radius $r$. The position of the bead relative to its predecessor is described by $\Theta$ (bond) and $\Phi$ (torsion) angles, which can vary according to the probability $p^*$. For example, if $p^* = 1$ all monomers have random values for $\Theta$ and $\Phi$ angle pairs. On the other hand, when $p^* = 0$, all monomer angle pairs have constant values and the polymer will form a rigid helical structure. Stiffness of the modelled polymer is regulated by narrowing the range of randomly chosen bond angle, by upper limit of $\Theta_{\mathrm{plim}}$. In the simulation 60,000 structures with different shape parameters ($\Theta_p$, $\Phi_p$, $\Theta_{\mathrm{plim}}$ and $p^*$) were modelled and for each structure the corresponding representative chain form factor $\bar{p(q)}$, radius of gyration $R_g$ and persistence length $l_p$ were calculated.

Non-charged polymer chains or segments of chains may attract each other and/or can form entanglements. Such interactions cause local inhomogeneities (so-called Debye–Bueche inhomogeneities) that lead to fluctuations in local density (Kajiwara & Miyamoto, 2005). This idea was originally introduced by Debye (1915) and was already successfully applied for the modelling of several polymer systems (Geissler et al., 1997; Horkay, Hecht, Zrínyi, & Geissler, 1996; Horkay, McKenna, Deschamps, & Geissler, 2000; Hecht, Horkay, & Geissler, 2001) including isolated extracellular polymeric substances and polysaccharides (EPS) (Dogsa et al., 2005; Draget, Stokke, Yuguchi, Urakawa, & Kajiwara, 2003). The scattering contribution is given by:

$$I(q) = \frac{\Delta\rho^2 8\pi\langle\delta\varphi^2\rangle\Xi^3}{(1+q^2\Xi^2)^2} \quad (3)$$

where $\Xi$ is the correlation length and $\langle\delta\varphi^2\rangle$ is the mean-square amplitude of the fluctuations of the local volume fraction of the polymer, which both describe the Debye–Bueche inhomogeneities. This term is often used as a summand with the simple Ornstein–Zernike term (Dogsa et al., 2005; Draget et al., 2003; Geissler et al., 1997; Horkay et al., 1996, 2000; Hecht et al., 2001) that is based on the correlation function of the ideal Gaussian chain in athermal solvents (de Gennes, 1979; Kajiwara & Miyamoto, 2005). In a similar manner we combined Eqs. (2) and (3) into total scattering function that was used for fitting the SAXS experimental data in this study:

$$I(q) = \Delta\rho^2\left[\frac{8\pi\langle\delta\varphi^2\rangle\Xi^3}{(1+q^2\Xi^2)^2} + \frac{\langle\varphi\rangle v_0}{1+Ke^{-q^2\xi^2}}P(\tilde{q})\right] \quad (4)$$

In the case of predominant repulsive interactions among the polymer chains (i.e. above the p$K_a$ of CMC), the macromolecules tend to distribute over the whole system rather homogeneously. Therefore the local density fluctuations, which can be represented by the variance of the volume fraction of the polymer $\langle\delta\varphi^2\rangle$, become insignificant ($\langle\delta\varphi^2\rangle = 0$) and Eq. (4) reduces to Eq. (2). In this case the parameter $K$ is positive, which indicates the presence of repulsive interactions. However, when repulsive interactions are not predominant (i.e. $K = 0$) and Debye–Bueche inhomogeneities are present in the system ($\langle\delta\varphi^2\rangle > 0$) Eq. (4) becomes Eq. (3) with an additional term $\Delta\rho^2\langle\varphi\rangle v_0 P(\tilde{q}) = \Delta\rho^2 c_N v_0^2 P(\tilde{q})$, where $c_N$ is the number density of polymer molecules in the sample. This term is due to the fine structure of the Debye–Bueche inhomogeneities. It is important to note that in the case of applying Eq. (3) alone or in the combination with Ornstein–Zernike term we did not obtain any acceptable fits to the experimental scattering curves. In such a system the form factor, $P(\tilde{q})$, reflects the average effective conformation of the polymer molecule or its segments of the size beyond which segments become uncorrelated inside the inhomogeneities. In our approach no assumption about chain shape is required (e.g. Gaussian ideal chain at certain length scale as by the Ornstein–Zernike term). In a trivial case, when $K = 0$ and $\langle\delta\varphi^2\rangle = 0$ no specific intermolecular interactions are present in the system and the scattering intensity according to Eq. (4) equals the representative form factor, $P(\tilde{q})$, of the polymer molecule. During the fitting procedure the interaction term was combined with all numerically calculated $P(\tilde{q})$ that represents different shapes of individual polymer chains. To account for smearing effects arising from the slit-collimation used in SAXS experiments, the first term on the right hand side of Eq. (4) can be analytically transformed to the form given by Dogsa et al. (2005) whereas the numerical smearing procedure can be applied to the second term.

In the present study the fitting range for the correlation length of the inhomogeneities, $\Xi$, was in the interval from 50 Å to 500 Å. Only solutions with $\Xi > 2R_g$ were accepted, because the size of dense domains which are built from CMC molecules cannot be smaller than twice the molecular radius of gyration. The fitting range for repulsion correlation length $\xi$ at different pH values was in the interval from 15 Å to 35 Å. For each tested correlation length value, the value of $K$, $\langle\varphi\rangle$ or $\langle\delta\varphi^2\rangle$ was estimated by solving Eq. (4) for the consecutive pairs of the first 100 points in the scattering curve. Estimates for electron density, $\rho$, were calculated by using an online scattering-length calculator (Munter, 2003). The volume of a single CMC molecule, $v_o$, having a $M_r$ of 82 kDa (dissociated form of CMC) and mass density of 1.45 g/cm$^3$, was calculated to be $10^{-19}$ cm$^3$.

### 2.5.2. Acceptable model solutions

In previous work (Dogsa et al., 2008) we used the root mean scaled standard deviation (RMSSD) as a measure of the quality of the fit. This measure of the fit quality does not take into account the differences in the distribution of densities in terms of points per unit of the reciprocal SAXS $q$-scale or real-space dimensions. For example, the $q$-scale has a constant resolution of 0.0005 Å$^{-1}$, meaning that from either $q = 0.01$ to 0.02 Å$^{-1}$ or $q = 0.10$ to 0.11 Å$^{-1}$ there are 20 points. However, the range of corresponding real-space dimensions in terms of Bragg distances are 300 Å and 50 Å, respectively. To correct for this, we modified the RMSSD by weighting it with the reciprocal of $q$. The weighted root mean scaled standard deviation (WRMSSD) was calculated as:

$$\mathrm{WRMSSD} = \sqrt{\sum_{i=1}^{k}\frac{1}{q_i}\frac{((m_i-d_i)/(s_i/\sqrt{n}))^2}{k\sum_{i=1}^{k}1/q_i}}, \quad (5)$$

where $m_i$ is the mean of the modelled $I(q)$ for each data point, $d_i$ is the mean of experimental $I(q)$ for each data point, $s_i$ is the standard deviation for each experimental $I(q)$ data point, $n$ is the number of data points contributing to $d_i$, and $k$ is the number of data points in the experimental scattering curve $I(q)$. This means that the difference between experimental and modelled scattering intensity $(m_i - d_i)$, is compared to the standard error of the experimental $I(q)$. During the fitting procedure the reciprocal $q$ weighted root mean scaled standard deviation (WRMSSD) is calculated for modelled scattering intensity of each conformation. The value of WRMSSD that is below unity indicates that the fitting curve has reached the fidelity of the experimental data, and all such fits are regarded as equally good. Therefore all chain conformations with WRMSSD $\leq 1$ were retained as equally probable solutions to the fitting problem within experimental error and are considered as acceptable model solutions. The number of acceptable solutions is not fixed in advance and depends on the quality of the experimental data and on the structural complexity of the system. With a larger range of experimental $q$ scale (especially in the regime of low $q$ values) and improved signal to noise ratio, a better resolution in solution space is achieved in terms of a lower number of acceptable results. In the case where the resulting molecular conformations do not differ enough, the fitting algorithm recognizes the corresponding form factors as indistinguishable. In this procedure no a priori assumptions about the conformation of the polymer molecule are made; the only criterion in accepting the solution is that WRMSSD $\leq 1$.

### 2.5.3. Calculation of radius of gyration and persistence length

On the basis of the structural parameters resulting from the string-of-beads model, the radius of gyration $R_g$ and the persistence length $l_p$ can be determined directly from the simulated molecular conformations. $R_g$ can be calculated using the distances $r_j$ of the $N$ monomers from the centre of mass:

$$R_g^2 = \frac{1}{N}\left\langle\sum_{j=1}^{N} r_j^2\right\rangle \quad (6)$$

The brackets denote the ensemble average, which in our case was calculated over 4000 conformations that were simulated for a specific set of shape parameters. Simultaneously, $l_p$ was calculated as the average projection of the end-to-end vector $\boldsymbol{s}_j$ on the bond vector $\boldsymbol{L}$ (Schäfer & Elsner, 2004) with the length of the monomer of 5.2 Å (Dogsa et al., 2008; Orehek et al., 2013).

### 2.5.4. Simulation of CMC supramolecular structure

Once the structural and interaction parameters were obtained by applying the string-of-beads model to the experimental SAXS data, the CMC supramolecular structure was simulated. To build a model of the CMC supramolecular structure the appropriate number of CMC molecules need to be grown in a simulation box obeying the periodic boundary conditions and taking into account their excluded volume. In addition, our model in Eq. (4) predicts intermolecular interactions, which are manifested in the non-uniform volume fraction of the polymer distribution across the simulation space. It turns out that in polymer gels a Gaussian distribution function is an adequate description of concentration fluctuations, with a mean volume fraction of the polymer $\langle\varphi\rangle$ and variance of $\langle\delta\varphi^2\rangle$ (Geissler, Hecht, Horkay, & Zrinyi, 1988; Hecht, Horkay, Mallam, & Geissler, 1992). To avoid the problem of negative concentrations a log-normal Gaussian distribution of the local-volume polymer fraction has been proposed (Hecht et al., 1992). We have therefore assumed a log-normal distribution of the local-volume fractions in CMC aqueous solution with mean $\mu$ and variance $\sigma^2$ calculated as:

$$\mu = \ln\left(\langle\phi\rangle\right) - \frac{1}{2}\ln\left(1 + \frac{\langle\delta\phi^2\rangle}{\langle\phi\rangle^2}\right) \tag{7}$$

$$\sigma^2 = \ln\left(1 + \frac{\langle\delta\varphi^2\rangle}{\langle\varphi\rangle^2}\right) \tag{8}$$

In principle one could model the entire distribution in one large simulation box, with a size exceeding the length over which the density fluctuations occur, $\Xi$. However, the density fluctuations in this case would be very difficult to observe in 3D space, because of large amount of polymer that becomes overcrowded in a large simulation box. Alternatively, the volume fraction distribution can be split into several sections, for which the average local polymer volume fraction $\varphi$ can be calculated. This average local $\varphi$ can be then represented in a smaller simulation box with size roughly corresponding to the correlation length, $\Xi$. In our case the log-normal distribution was arbitrarily split into five sections: extremely low $\varphi$ (5%), low $\varphi$ (15%), medium $\varphi$ (60%), high $\varphi$ (15%), and of extremely high $\varphi$ (5%) volume fraction, where the percentage indicates the fraction of the total CMC sample space occupied with the given local volume fraction. The density fluctuations (i.e. Debye–Bueche heterogeneities) that result in scattering of X-rays, as given by Eq. (3), are typically caused by polymer entanglements or local aggregates, which are of size of a ten to a few tens of nm. In Fig. 2 representative individual polymer structures that may form the Debye–Bueche heterogeneities when neighbouring polymers entangle or form aggregates are depicted. The presentation of Debye–Bueche heterogeneities in real space, consisting of a collection of structures depicted in Fig. 2 is given in Fig. 3 (for pH 1.6 and 3.6). The correlation length of Debye–Bueche heterogeneities was 33 nm (the dimension of a box in Fig. 3). Each box represents the Debye–Bueche heterogeneities of a certain polymer density. The polymer density distribution is given at the top of Fig. 3.

## 2.6. Evaluation of DLS results

In the dynamic light scattering experiments the fluctuations of the scattering intensity with time are monitored and are usually

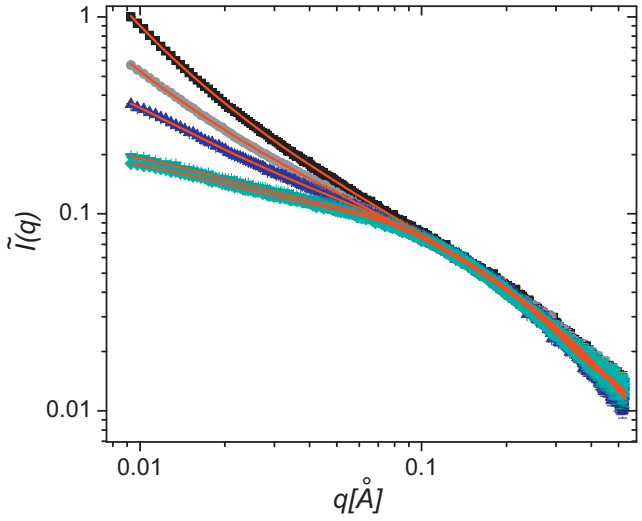


**Fig. 1.** Log–log plots of experimental SAXS intensities of 2.0% (w/v) CMC at different pH values: 1.6 (■), 3.1 (●), 3.6 (▲), 5.0 (▼), and 7.0 (◆). Due to the line-collimated primary X-ray beam in SAXS camera, these results are experimentally smeared. The scattering curves were normalized to coincide in the region of high $q$ values. Red lines represent best fits to the data by the string-of-beads model (Eq. (4)). (For interpretation of the references to colour in this figure legend, the reader is referred to the web version of the article.)

expressed in a form of experimentally accessible intensity autocorrelation function $G_2(\tau)$, which is connected to the scattering amplitude (field) autocorrelation function $G_1(\tau)$ via well-known Siegert relation (Berne & Pecora, 2000):

$$G_2(\tau) = B + C[G_1(\tau)]^2, \tag{9}$$

where parameter $B$ is the baseline and constant $C$ represents the strength of the coherent signal. The DLS data of the polymer solutions that show a pronounced bimodal shape of the $G_2(\tau)$ function can be appropriately described by mode coupling theory (Hoffmann et al., 2011; Kjøniksen, Nilsson, Thuresson, Lindman, & Nyström, 2000; Kjøniksen, Nyström, & Lindman, 1998; Nyström, Kjøniksen, & Iversen, 1999; Rajagopal, Ngai, & Teitler, 1991). This approach predicts the system of small primary scattering units that exhibit fast dynamics of the diffusive character, but due to their weak or moderate interaction (coupling) between each other or their surrounding cause an additional retarded relaxation process that is usually much slower. A comprehensive mode coupling theory (Ngai, Rajagopal, & Lodge, 1990; Ngai, Rajagopal, Rendell, & Teitler, 1986; Ngai, Rajagopal, & Teitler, 1988) leads to the following expression for the $G_1(\tau)$ function:

$$G_1(\tau) = A_f \cdot e^{-\tau/\tau_f} + A_s \cdot e^{-(\tau/\tau_{se})^{\beta}}, \tag{10}$$

with $A_f + A_s = 1$ representing the amplitudes for fast and slow relaxation mode, respectively, $\tau_f$ being the relaxation time of the fast mode, $\beta$ the parameter connected to the coupling parameter $n$ via $\beta = 1 - n$ and $(0 < \beta \leq 1)$, and $\tau_{se}$ some effective relaxation time of the slow mode. One can get the mean relaxation time of the slow mode according to the following expression:

$$\tau_s = \int_0^{\infty} e^{-(\tau/\tau_{se})^{\beta}}\, dt = \frac{\tau_{se}}{\beta}\Gamma\left(\frac{1}{\beta}\right), \tag{11}$$

where $\Gamma(\beta^{-1})$ is the gamma function of $\beta^{-1}$. It is expected that fast relaxation time, will show $q^{-2}$ dependence if the process is diffusive. Combining Eqs. (9) and (10) allows for the determination of the

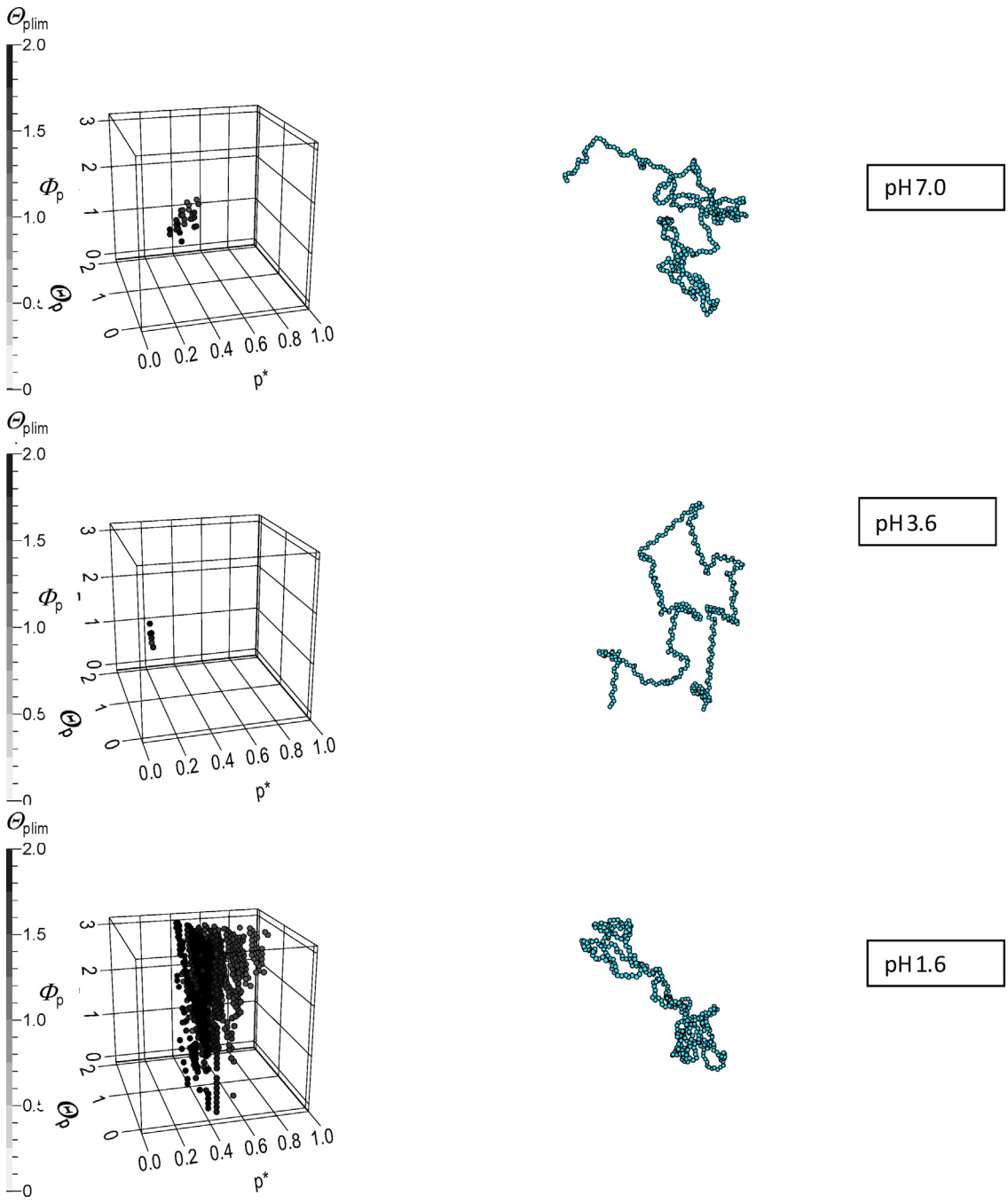


**Fig. 2.** Model shape parameters and representative structures of CMC at different pH values. Shape parameters are presented in four dimensions: $p^*$, probability of a monomer with a random $\Theta$ (bond) and $\Phi$ (torsion) angles, where $\Theta$ is limited by $\Theta_{plim}$. With probability $(1-p)$, the monomer will have a $\Theta = \Theta_p$ and $\Phi = \Phi_p$. Each point in a solution space is a solution of the fitting algorithm that gave equally good fit (i.e. WRMSSD $\leq 1$). The conformation of the best fit solution is depicted on the right hand side of the figure with the corresponding fitting parameters: 0.5, 0.9, 1.2 [rad] for $\Theta_p$, 1.1, 1.2, 1.9 [rad] for $\Phi_p$, 2.0, 1.75, 1.25 [rad] for $\Theta_{plim}$, and 0.30, 0.15, 0.45 for $p$ at pH 7.0, 3.6 and 1.6 respectively.

parameters of Eq. (11) from the experimental DLS data. Decreasing value of $\beta$ indicates increasing coupling in the system.

### 2.7. Theoretical viscosity calculations

The calculations of theoretical intrinsic viscosities were based on the persistent cylinder model of Yamakawa and Fujii (1974), which has been already successfully applied to the cellulose derivatives (Dayan, Maissa, Vellutini, & Sixou, 1982). The model takes into account the length of the polymer which is 2080 Å (i.e. for DP = 400, and the monomer length of 5.2 Å), the molecular mass of CMC ($M_w$ of CMC = NaCMC − Na = 82 kDa), the diameter (5.2 Å) and the persistence length $l_p$, which was taken from the string-of-beads model simulations.

### 2.8. Microscopy

For microscopic examination 10 μL of CMC solution was transferred to a microscope slide and covered by a glass coverslip. The images were taken under a Zeiss Axio Observer Z1 inverted microscope, equipped with a Mrm Axiocam camera using the phase contrast technique. A total magnification of 1000× was used.

**Table 1**
Interaction parameters of the fits to the experimental SAXS data and calculated parameters of 2% (w/v) CMC at different pH values. Parameters corresponding to Gaussian repulsion interaction: $\xi$ is repulsion interaction correlation length, and $K$ is constant proportional to polymer concentration and strength of interactions. Parameters corresponding to Debye–Bueche interaction mode: $\Xi$ is the correlation length describing the size of heterogeneous regions, and $\langle\delta\varphi^2\rangle/\langle\varphi\rangle^2$ is the relative volume fraction fluctuation of the polymer within the system. The ranges of parameter values of good fits are given, with numbers in bold denoting the values of the best fits. The pH dependence of radius of gyration, $R_g$, and persistence length, $l_p$ as calculated from polymer structures simulated by string of beads model. Intrinsic viscosity [$\eta$] was calculated by Yamakawa model (Yamakawa & Fujii, 1974).

| | CMC at pH 7.0 | CMC at pH 5.0 | CMC at pH 3.6 | CMC at pH 3.1 | CMC at pH 1.6 |
|---|---|---|---|---|---|
| Interaction fitting parameters | | | | | |
| $\xi$ [Å] | 20–**20**–23 | 20–**23**–25 | 0 | 0 | 0 |
| $K$ | 2.3–**2.5**–2.7 | 1.4–**1.5**–2.1 | 0 | 0 | 0 |
| $\langle\delta\varphi^2\rangle/\langle\varphi\rangle^2$ [a] | 0 | 0 | 0.4–**0.45**–0.5 | 1.6–**1.7**–1.9 | 3.7–**4.0**–6.0 |
| $\Xi$ [Å] [b] | 0 | 0 | 320–**320**–500 | 260–**280**–470 | 220–**230**–300 |
| Calculated parameters | | | | | |
| $l_p$ [Å] | 36-**40**–51 | 40-–**60**–60 | 69-**71**–71 | 45–**49**–54 | 30–**35**-–39 |
| $R_g$ [Å] | 110–**116**–127 | 117-**142**–142 | 150–**154**–156 | 125–**128**–134 | 99–**108**-–115 |
| [$\eta$] [$dl/g$] | 1.1-**1.3**–1.7 | 1.3–**2.0**–2.0 | 2.1–**2.1**–2.1 | 1.5–**1.6**–1.8 | 1.0–**1.1**–1.3 |

[a] Assumptions: $V(\text{single chain}) = 10^{-19}\ \text{cm}^3$, $\rho(H_2O) = 9.46 \times 10^{-6}\ \text{cm}^{-2}$, $\rho(\text{polymer}) = 1.30 \times 10^{-6}\ \text{cm}^{-2}$.
[b] Assumption: $\Xi > 2R_g$.

### 2.9. Density and sound velocity measurements

The densities and sound velocities of CMC solutions were measured using a DMA 5005 (prototype instrument; Anton Paar, Graz) equipped with a sound velocity measuring cell. The corresponding adiabatic compressibility values were calculated according to the well-known Laplace equation $\beta_S = 1/(v^2\rho)$, where $v$ is the velocity of sound in the solution and $\rho$ the density of the solution. The hydration numbers $n_h$ were then calculated from these data based on the Pasynski model (Burakowski & Glinski, 2010, 2012; Glinski & Burakowski, 2013).

## 3. Results

### 3.1. SAXS results

Small-angle X-ray scattering intensities of 2% (w/v) CMC samples at different pH values and at a constant ionic strength are shown in a double logarithmic plot in Fig. 1.

These scattering curves suggest a strong pH dependence, especially at scattering vectors $q < 0.15\ \text{Å}^{-1}$ corresponding to Bragg distances of $d > 40$ Å. The slopes of the scattering curves in this region increase with decreasing pH, indicating the presence of pH dependent supramolecular structures. The scattering curve at pH 3.6 represents the system at the p$K_a$ value of CMC in aqueous solution, which was estimated to be 3.65 (King & Smibert, 1963). The generalized string-of-beads model (Eq. (4)) was applied to the SAXS scattering data and the corresponding fits are shown in Fig. 1. All fits that have reached the fidelity of the experimental data (i.e. WRMSSD < 1) comprised a population of equally acceptable solutions within the experimental error. These fitting solutions for shape parameters for CMC solubilized at pH 7.0, 3.6, and 1.6 are depicted in Fig. 2 in the form of 3D cubes with the fourth dimension represented as a greyscale. The corresponding range of interaction parameters at different pH values is given in Table 1.

As indicated in Fig. 2, the molecular structure of CMC was pH dependent. The CMC-molecular conformation was most expanded around p$K_a$. This was indicated by the low $p$ value. On average only 15% of all monomers forming the CMC molecule had random values of $\Theta$ and $\Phi$. All the other monomers had fixed $\Theta$ and $\Phi$ values of $\Theta_p$ and $\Phi_p$ forming long helical segments. At p$K_a$ highest $R_g$ and $l_p$ values were obtained. At pH 1.6 the CMC chains were practically uncharged and an increase in parameter $p$ (centred at $p = 0.5$) was observed. The ratio of $\Phi_p/\Theta_p$ for equally good fits was higher than 2/3, suggesting the presence of compact helical segments in the molecular structure. The population of equally good fits increased compared to pH 3.6. The broader distribution of solutions at pH 1.6 is likely a consequence of decreased sensitivity of $\Theta_p$, $\Phi_p$ at higher $p$ values. For example, at $p = 1$ all monomers have a random value of $\Theta$, $\Phi$ and therefore changes of $\Theta$, $\Phi$ cannot be structurally distinguished.

Single CMC molecular chains interact with each other in solution. As given in Table 1, the strongest repulsion interactions, $K$, were obtained at neutral pH, where practically all carboxymethyl groups on CMC were dissociated. The repulsion correlation length, $\xi$, was around 20 Å. Around p$K_a$ the repulsive forces decreased considerably and segregation of molecular chains occurred. This is parameterized by a relative volume fraction fluctuation of the polymer $\langle\delta\varphi^2\rangle/\varphi^2$, which describes the heterogeneity of the system. Volume fraction fluctuations of the polymer increased with decreasing pH. At the same time the correlation length, $\Xi$, which describes the distance over which on average the local density inhomogeneities extend, decreased at low pH.

Supramolecular CMC structures at different values of pH are presented in Fig. 3. The supramolecular structure of CMC solution was simulated on the basis of the log-normal distributions of CMC number density obtained from $\langle\delta\varphi^2\rangle/\varphi^2$ as shown in Table 1. For instance, subspaces denoted by $\varphi_{60\%}$ in Fig. 3 represent the characteristic subspace polymer distribution that can be found in approximately 60% of the CMC sample volume. The results of supramolecular simulation suggest that at pH 7.0 the distribution of CMC molecules was rather homogeneous throughout different subspaces. At pH 3.6 the spatial polymer distribution was skewed to the right, suggesting that the CMC supramolecular structure was less homogeneous and more tightly packed. Furthermore, the distribution at pH 1.6 was profoundly asymmetric, with most CMC chains found in denser subspaces, where they form dense aggregates. Across the given subspace, as well as along a given pH, substantial differences were observed in the CMC supramolecular structure as depicted in Fig. 3.

The results for SLS and DLS measured at the scattering angle of 90° are shown in Fig. 4 and complement the SAXS results. A strong increase in the scattering intensity was observed for the CMC samples with pH values below 3.6 (Fig. 4a). In the case of particulate systems the light scattering intensity scales with the sixth power of the particle-radius. If CMC behaves as a particulate system, this would indicate the presence of large scattering particles at lower pH values. However, one has to be cautions when speaking about particles in such systems containing long polymer molecules, because these systems are not necessarily particulate; instead larger formations of entangled polymer molecules, which can extend over the sample volume, can form in such samples.

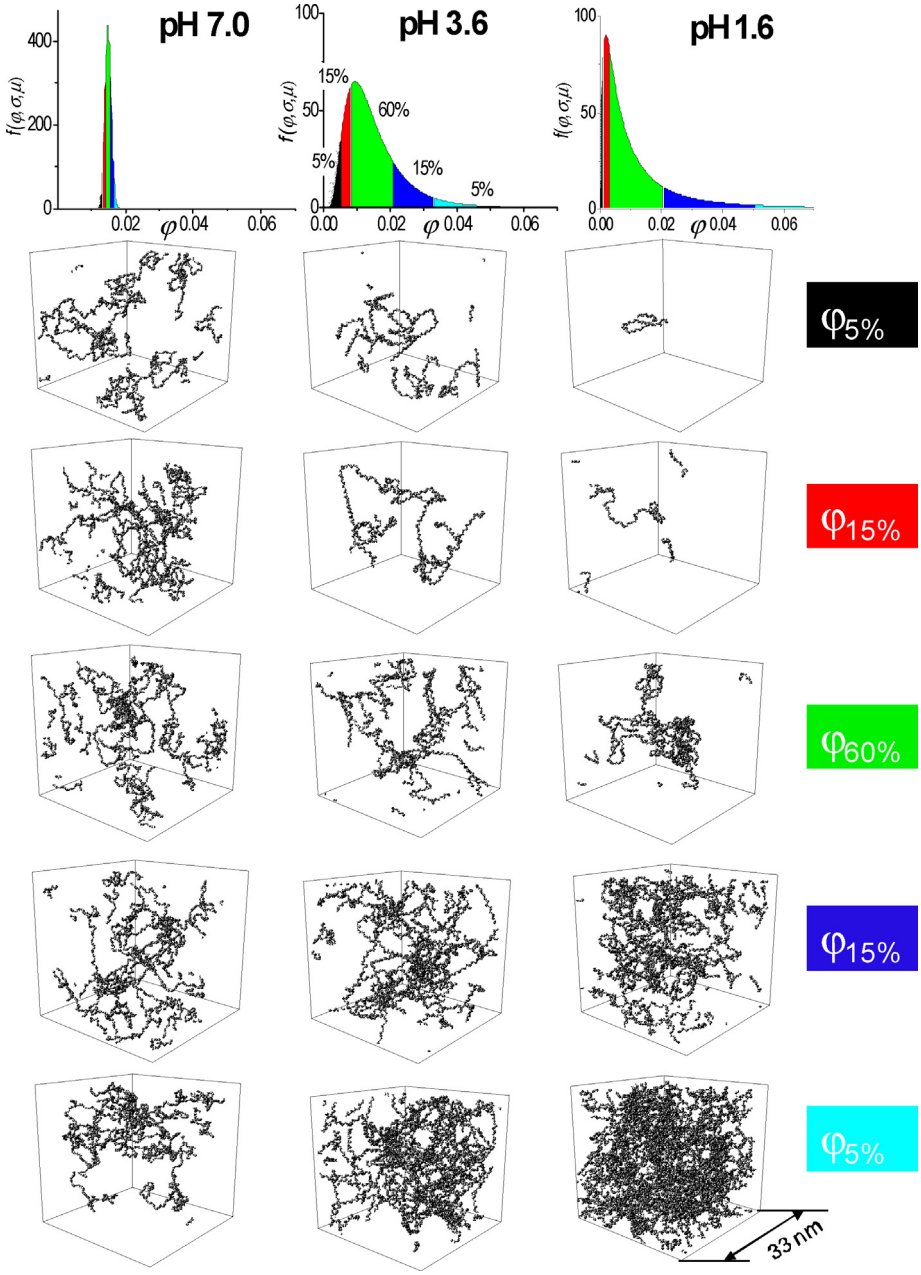


**Fig. 3.** Representation of CMC molecular distribution in space, calculated on the basis of the resulting interaction parameters presented in Table 1 and the best-fit shape parameters from Fig. 2. The size of the monomer bead (5.2 Å) is depicted in proportion to the side-length of the subspace box (330 Å). These subspaces were obtained on the basis of the log-normal chain-density distributions defined by the average value $\langle\varphi\rangle = 0.013$ and the average fluctuations $\langle\delta\varphi^2\rangle = 6.76 \times 10^{-4}$, $8.37 \times 10^{-5}$, for pH 1.6 and 3.6, respectively. For pH 7, where the fitting solutions were obtained for repulsive interaction only, the $\langle\delta\varphi^2\rangle$ was assumed to be $8.37 \times 10^{-7}$. On the right-hand side of the figure the index of $\varphi$ denotes the probability to encounter a characteristic subspace with the local $\varphi$ in a CMC sample at a given value of pH.

Nevertheless, as shown in Fig. 5, the appearance of some dense highly polydisperse CMC particles was actually observed with microscopy in the size regime of a few 100 of micrometers at pH 1.6 but not at pH 7.0.

The DLS intensity autocorrelation function $G_2(\tau)$ shown in Fig. 4b clearly shows a bimodal form at high values of pH. This indicates the presence of at least two relaxation processes with very different relaxation times. In particulate system this would mean the presence of two populations of scattering particles with very different particle sizes. With decreasing value of pH, the bimodal shape of the $G_2(\tau)$ function gradually becomes progressively less evident (Appendix B). In addition, the $G_2(\tau)$ function gradually shifts toward longer delay times $\tau$. These results are therefore in full agreement with the SLS results that indicate a strong increase in the size of the scattering structures at low value of pH.

For a detailed evaluation of the DLS results we followed the DLS data evaluation protocol established for polymer solutions showing a bimodal $G_2(\tau)$ function, i.e. mode coupling theory. To test the diffusive character of the samples additional DLS measurements were performed at scattering angles between 80° and 140°. Such measurements detect dynamics (relaxation processes) on different length scales which correspond to various values of the scattering vector $q$.

The results of the mode coupling approach for fast and slow component are presented in a reduced form in Fig. 6. The two modes observed in DLS experiments (slow and fast) have very different

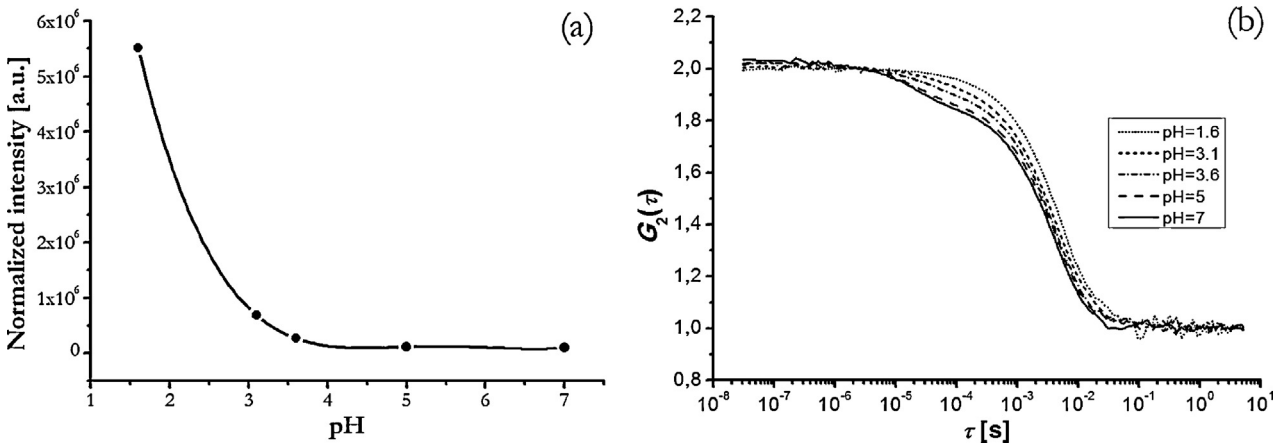


**Fig. 4.** Static Light scattering results for 2% (w/v) aqueous solution of CMC measured at the scattering angle of 90°. (a) pH dependence of the normalized SLS intensity. (b) DLS intensity autocorrelation function $G_2(\tau)$.

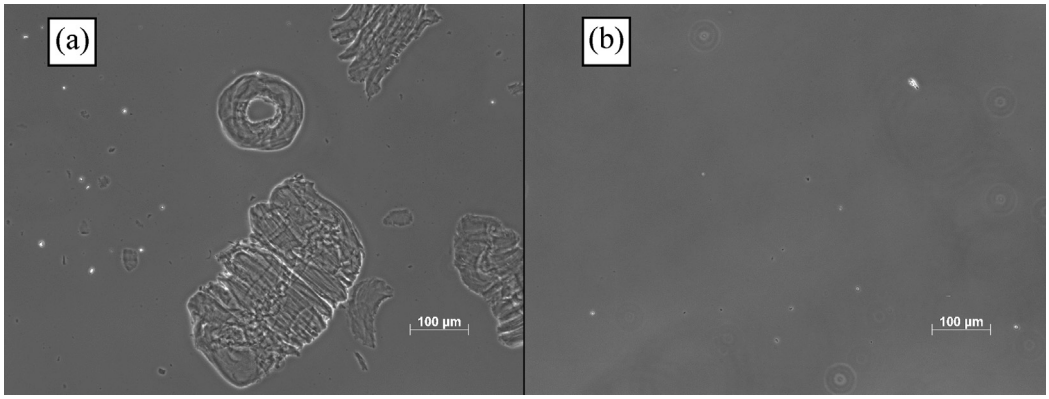


**Fig. 5.** Phase contrast microscopy of 2% (w/v) aqueous solutions of CMC at pH value of 1.6 (a) and 7.0 (b).

origin as indicated by the $\ln(1/\tau_1)$ versus $\ln(q)$ plots. Whereas fast relaxation mode is diffusive in character the slow is non-diffusive and arises from the mode coupling due to the interparticle interactions and polymer entanglements. The slopes of $\ln(1/\tau_1)$ versus $\ln(q)$ (Fig. 6a) for CMC at pH above p$K_a$ are approximately equal suggesting similar relaxation mode. On the other hand, the slope at pH below p$K_a$ is bigger suggesting more compact polymer conformations. The results suggest that some parts in the CMC structure behave as fast diffusive-type moieties that may interact between each other and become entangled resulting in much slower non-diffusive relaxation mode. As given in Fig. 6c the entanglement becomes pronounced around p$K_a$ of CMC and dominates the CMC suprastructure at low pH values. There are two regimes for CMC macromolecular structure, predominantly non-entangled at high pH and entangled at low pH with a quick transition around the p$K_a$ value.

### 3.2. Viscosity measurements

The results of viscosity measurements at different CMC pH values are shown in Fig. 7a. The viscosity increased non-linearly with increased CMC concentration. The viscosity was highest at neutral pH and decreased at low pH. The results for the intrinsic viscosity are given in Fig. 7b. In the limit of infinite dilution there are two states of viscosity behaviour. At low pH the intrinsic viscosity is low. There is a sharp transition around p$K_a$ to high intrinsic viscosities at high pH values. To study hydration of carboxymethyl polymers at different pH values density and sound velocity of CMC solutions were measured. The results enabled us to calculate the adiabatic compressibility that was used in turn to determine hydration numbers of CMC. The relative change of compressibility due to bound water in hydration spheres, can be used to obtain the hydration number, by Pasynski equation (Burakowski & Glinski, 2010). The results indicate an increased sample density and speed of sound at higher pH values. Consistently the hydration numbers increased with pH. This is consistent with more expanded CMC structure at higher pH. However, the effect of pH on hydration number at different pH was small (see Appendix C).

The pseudoplastic behaviour of CMC at different pH values is shown in Fig. 8. Depending on pH, different flow behaviour of CMC was observed. At low pH a pronounced shear-thinning was observed, where the apparent viscosity decreased with increasing shear rate. Above the p$K_a$, the effect of shear-thinning was less pronounced.

## 4. Discussion

CMC is arguably the most frequently used polymer in industrial applications. Despite several decades of extensive research its supramolecular structure in solution is not well characterized. In this work SAXS, DLS, SLS, microscopy and viscosimetry were used to examine the supramolecular structure of aqueous solutions of CMC

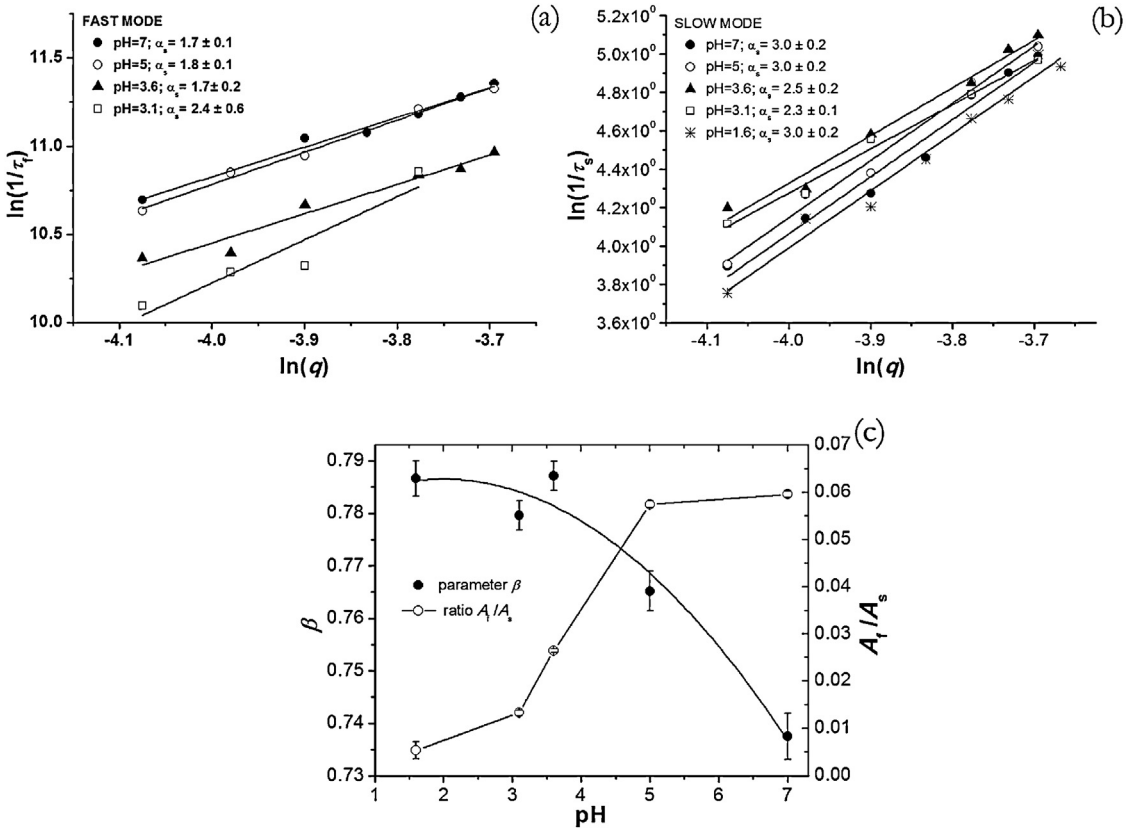


**Fig. 6.** Fast (a) and slow relaxation component (b) in DLS experiments at different pH values. Linear fits with the slopes, $\alpha_s$, in the inset are given. (c) pH dependence of the parameter $\beta$ and the ratio $A_f/A_s$ obtained from the coupling mode analysis.

at different pH values. To visualize CMC supramolecular structure at different pH values the information from SAXS results was combined with light scattering and rheology experiments to simulate the number density distribution of individual molecules in different volume subspaces of CMC sample.

The results of the SAXS, SLS, DLS, viscosity measurements and microscopy clearly indicate a profound structural response of the polymer around the p$K_a$ value of CMC. The results can be summarized as follows. Below the p$K_a$ there was a significant increase in density fluctuations of the polymer, which lead to the formation of dense aggregates of CMC molecules. The static light scattering intensity increased profoundly, which is consistent with the presence of dense large scatterers observed by microscopy and SAXS. At the nanoscale, the SAXS results indicate a micro phase-separation in the form of strong inhomogeneities in the supramolecular structure. Micro phase-separation gave rise to gradually decreased coupled relaxation dynamics consistent with polymer aggregation and entanglement. As a result of micro separation viscosity of the CMC solution significantly decreased. At pH values above p$K_a$ the SAXS results indicate partially expended CMC structure with strong electrostatic repulsion between neighbouring CMC chains. The bimodal shape of the DLS intensity autocorrelation function observed above the p$K_a$ value indicates a rather complex relaxation dynamics composed of fast and slow relaxation dynamics.

The reason for the micro phase-separation below p$K_a$ lies in the lack of repulsion between neighbouring CMC chains, which enables formation of very dense CMC packing. The correlation length describing the size of heterogeneous regions, $\Xi$, steadily decreases upon reducing the pH value from 3.6 to 1.6. At low

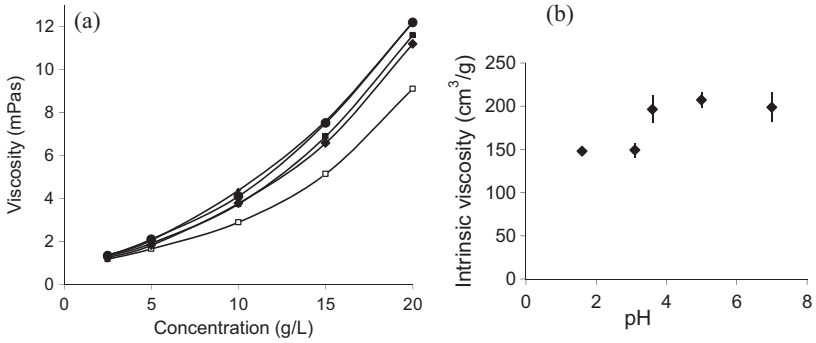


**Fig. 7.** (a) Concentration dependence of viscosity for CMC at different pH values: pH 7 (■), pH 5 (●), pH 3.6 (▲), pH 3.1 (♦) and pH 1.6 (□). (b) Intrinsic viscosities of CMC solutions in 0.1 M electrolyte (NaCl/HCl) at different pH values with estimated errors.

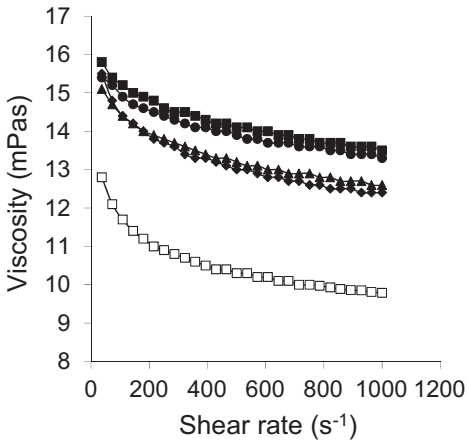


**Fig. 8.** Flow curves of 2% (w/v) CMC at pH 7 (■), pH 5 (●), pH 3.6 (▲), pH 3.1 (♦) and pH 1.6 (□).

pH values the spatial distribution of CMC is heterogeneous–the significant part of the sample volume is dilute or even devoid of CMC molecules. On the other hand, the majority of the CMC molecules are concentrated into high density regions. These facts have consequences for the dynamics for both fast and slow relaxation processes. With decreasing pH the slow relaxation mode obviously predominates in the dynamics of the sample. These can be explained by increased incorporation of individual chains into the dense larger regions, which is consistent with the results from SAXS results and modelling.

CMC is a polyelectrolyte with a p$K_a$ value of 3.65. At p$K_a$, the CMC molecular structure is maximally expanded as indicated by the largest $R_g$ and $l_p$ values. With decreased pH the carboxymethyl groups of the polymer become predominantly uncharged. Decreasing the charge of the polymer lowers its propensity to expand. In agreement with this are the results of SAXS modelling, indicating more random molecular structure. Accordingly, $R_g$ and $l_p$, are lowered. Below the p$K_a$ value of CMC the intrinsic viscosity is lowered as well. When pH is increased above p$K_a$ carboxymethyl groups become progressively charged. SAXS results show strong long-range repulsive interactions at high values of pH and at the same time the highest sample and intrinsic viscosities are present at these conditions. The intrinsic viscosities can be independently obtained from Yamakawa model (Yamakawa & Fujii, 1974) utilizing the $l_p$ obtained by SAXS. Below the p$K_a$ the two intrinsic viscosities agree. However, above the p$K_a$ the calculated and experimentally obtained intrinsic viscosities disagree. The reason for this apparent discrepancy is the relatively high concentration of CMC in the samples used for SAXS measurements (2% CMC) from which $l_p$ was obtained. High concentration in samples appreciably differs from the extrapolated zero concentration, which is used for determination of the intrinsic viscosity. At high pH the expansion of individual polymer chains driven by intramolecular repulsion is counterbalanced by intermolecular repulsion in the system, preventing full polymer expansion. Therefore the $l_p$ value obtained from SAXS measurements is lower compared to dilute solutions. The apparent discrepancy in $l_p$ obtained from SAXS and intrinsic viscosity measurements can therefore be regarded as a measure of intermolecular repulsion and should correlate with the strength of the repulsion parameter $K$. This was indeed observed; at pH 3.6 where the calculated and observed intrinsic viscosities exactly match is repulsion parameter $K$ equal to zero.

Intermolecular repulsion potential should therefore have an effect on supramolecular structure and dynamics. The effect can be seen from the results of viscosity measurements at different pH values. As already noted by Kästner et al. (1997), at pH < 3 the viscosity of CMC is decreased, which is in agreement with our results. At pH 1.6 locally compact high-density suprastructure is formed, which results in a low overall sample viscosity. In addition, a high degree of shear-thinning was observed. The supramolecular structure at low pH with entangled compact CMC structures allows easier orientation and deformation of polymers in the direction of flow upon applying shear stress. Preferential orientation along flow lines reduces system viscosity at high shear rate. On the other hand, at pH 7.0, the individual CMC chains are expanded and negatively charged. Stronger repulsion increases polymer stiffness causing more friction, which increases sample viscosity and decreases the amount of shear-thinning. This suggests that the charged CMC polymer chains are not easily oriented and deformed in the direction of flow upon increasing shear stress. Even at the highest shear rate applied, the viscosity of CMC at pH 7.0 was significantly higher than the viscosity at pH 1.6 at very low shear rates. This emphasizes the very important role of repulsive interactions in CMC systems at pH values above p$K_a$.

Modelling supramolecular structures of CMC is not an easy task (Schulz, Burchard, & Dönges, 1998). No lesser challenge is a representation of the complex 3D geometrical supramolecular model in 2D plane. In this work the amorphous supramolecular structure of CMC is described as a non-homogenous expanded network that contains a large number of voids of approximately the size of the CMC molecule or larger. The suprastructure is represented as a collection of five characteristic subspaces with different molecular densities. The representation is based on the log-normal number density distribution defined by the average value $\langle\varphi\rangle$ and its average fluctuations $\langle\delta\varphi^2\rangle$. From the results depicted in Fig. 3 it is obvious that the distribution of CMC molecules in different density subspaces varies strongly with pH. Narrow distribution at pH 7.0 indicates that CMC molecules are approximately homogenously distributed through the sample volume. On the other hand, a highly skewed distribution at low pH suggests that a significant fraction of the sample volume is not populated with CMC. Due to extreme packing density the majority of CMC molecules are packed in dense entangled aggregates that occupy only 20% of the total sample volume. Such a picture is consistent with the results of the dynamic light scattering. As the majority of the CMC molecules are in dense aggregates only one mode of relaxation is observed; the slow relaxation time of the entangled globules of polymer molecules. On the other hand, at high pH one can observe individual molecules that form a meshlike polymer network. Two relaxation times were observed. Fast diffusive, consistent with free molecules and slow indicative of network dynamics. Although network relaxation was slow it was faster than slow relaxation time observed for globules of entangled polymer molecules indicating that the two processes are different. At around p$K_a$ value CMC polymer molecules have the smallest interaction potential as suggested by the most expended CMC structure, shortest slow relaxation times, and smallest SAXS interaction parameters.

## 5. Conclusions

It is rewarding to see that the results of different techniques employed in this study, SAXS, SLS, DLS, microscopy, and viscosity measurement combined with modelling give coherent picture of structural behaviour of CMC in aqueous solutions at different pH values. The information gathered by different techniques enables one to visualize structural information on a large spatial scale from 1 nm to 100 μm and correlates structure to function via dynamical behaviour of the polymer solution. Having information on such a large spatial window is crucial for understanding of many biological and industrial processes where CMC or other carbohydrates are

used. The approach developed in this study allows one to develop a much better intuition about the supramolecular structure and behaviour of carbohydrate solutions.

## Acknowledgements

We acknowledge the financial support of the Slovenian Research Agency through the Physical Chemistry Programme Group P1-0201 and Microbiology and biotechnology of food and environment Programme Group P4-0116.

## Appendix A.

See Fig. A1.

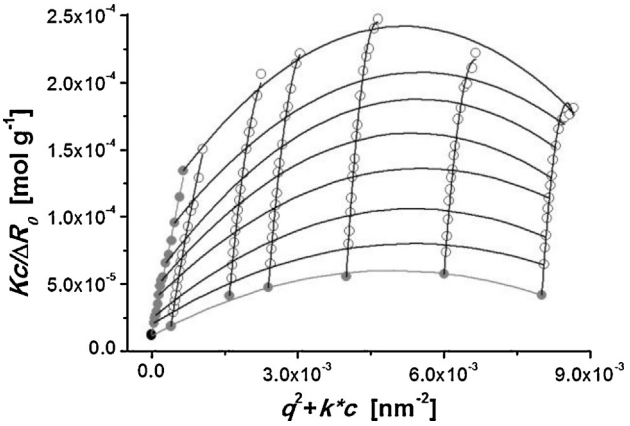


**Fig. A1.** Basic characterization of the CMC polymer: (a) SLS results for the CMC solutions from 0 5 mg mL$^{-1}$ to 10 mg mL$^{-1}$ for the scattering angles from 30° to 150° in a form of the Zimm diagram.

## Appendix B.

See Fig. B1.

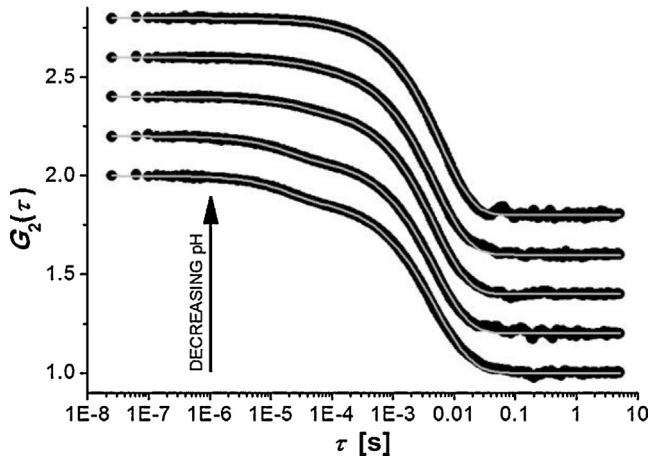


**Fig. B1.** Fits of the mode coupling evaluation approach for the $G_2(\tau)$ function measured at the scattering angle 90° and various values of pH for 7 to 1.6. The curves are shifted upwards by ($n \times 0.2$) for the sake of visibility.

## Appendix C.

See Fig. C1.

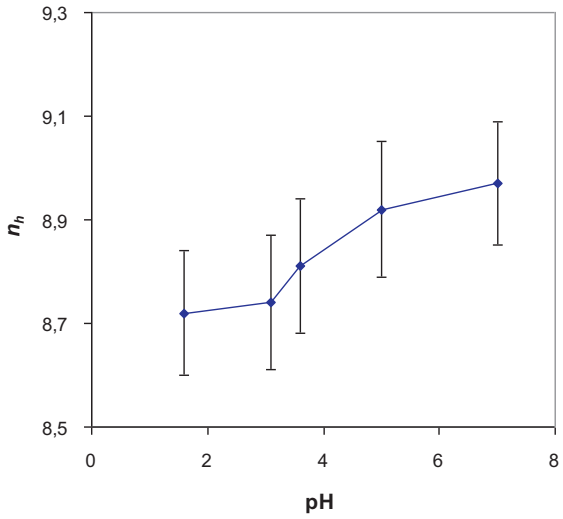


**Fig. C1.** Hydratation number of CMC $M_w$ = 90 kDa, DS = 0.7 at 20 °C.

## References

Adel, A. M., Abou-Youssef, H., El-Gendy, A. A., & Nada, A. M. (2010). Carboxymethylated cellulose hydrogel. Sorption behavior and characterization. *Nature and Science*, *8*, 244–256.

Benchabane, A., & Bekkour, K. (2008). Rheological properties of carboxymethyl cellulose (CMC) solutions. *Colloidid and Polymer Science*, *286*, 1173–1180.

Berne, B. J., & Pecora, R. (2000). *Dynamic light scattering with applications to chemistry, biology, and physics*. New York: Dover Publications.

Brown, W., & Mortensen, K. (2000). *Scattering in polymeric and colloidal systems*. Amsterdam: Overseas Publishers Association.

Burakowski, A., & Glinski, J. (2012). Hydration numbers of nonelectrolytes from acoustic methods. *Chemical Reviews*, *112*, 2059–2081.

Burakowski, A., & Glinski, J. (2010). Hydratation numbers of non-elecrolytes in aqueus solvents of fixed pH. *Interntional Journal of Termophysics*, *31*, 16–25.

Clasen, C., Plog, J. P., Kulicke, W.-M., Owens, M., Macosko, C., Scriven, L. E., et al. (2006). How dilute are dilute solutions in extensional flows? *Journal of Rheology*, *50*, 849–881.

Cummings, J. H., & Stephen, A. M. (1979). Water-holding by dietary fibre in vitro and its relationship to faecal output in man. *Gut*, *20*, 722–729.

Coviello, T., Maeda, H., Yuguchi, Y., Urakawa, H., Kajiwara, K., Dentini, M., et al. (1998). Conformational characteristics of oxidized scleroglucа. *Macromolecules*, *31*, 1602–1607.

Dayan, S., Maissa, P., Vellutini, M. J., & Sixou, P. (1982). Intrinsic viscosity of cellulose derivatives and the persistent cylinder model of Yamakawa. *Polymer*, *23*, 800–804.

de Gennes, P. (1979). *Scaling concepts in polymer physics*. New York: Cornell University Press.

Debye, P. (1915). Zerstreuung von röntgenstrahlen. Scattering from non-crystalline substances. *Annalen der Physik*, *46*, 809–823.

Dogsa, I., Kriechbaum, M., Stopar, D., & Laggner, P. (2005). Structure of bacterial extracellular polymeric substances at different pH values as determined by SAXS. *Biophysical Journal*, *89*, 2711–2720.

Dogsa, I., Štrancar, J., Laggner, P., & Stopar, D. (2008). Efficient modeling of polysaccharide conformations based on small-angle X-ray scattering experimental data. *Polymer*, *49*, 1398–1406.

Doutch, J., Bason, M., Franceschini, F., James, K., Clowes, D., & Gilbert, E. P. (2012). Structural changes during starch pasting using simultaneous Rapid Visco Analysis and small-angle neutron scattering. *Carbohydrate Polymers*, *88*, 1061–1071.

Doutch, J., & Gilbert, E. P. (2013). Characterisation of large scale structures in starch granules via small-angle neutron and X-ray scattering. *Carbohydrate Polymers*, *91*, 444–451.

Draget, K. I., Stokke, B. T., Yuguchi, Y., Urakawa, H., & Kajiwara, K. (2003). Small-angle X-ray scattering and rheological characterization of alginate gels. 3. Alginic acid gels. *Biomacromolecules*, *4*, 1661–1668.

Emeje, M. O., Kunle, O. O., & Ofoefule, S. I. (2006). Effect of the molecular size of carboxymethylcellulose and some polymers on the sustained release of theophylline from a hydrophilic matrix. *Acta Pharmaceutica*, *56*, 325–335.

Geissler, E., Hecht, A. M., Horkay, F., & Zrinyi, M. (1988). Compressional modulus of swollen polyacrylamide networks. *Macromolecules*, *21*, 2594–2599.

Geissler, E., Horkay, F., Hecht, A. M., Rochas, C., Linder, P., Bourgaux, C., et al. (1997). Investigation of PDMS gels and solutions by small angle scatterin. *Polymer*, *38*, 15–20.

Glinski, J., & Burakowski, A. (2013). Modification of the Pasynski Method for determining the hydration numbers of nonelectrolytes. *Chemical Physics Letters*, *566*, 21–24.

Hecht, A. M., Horkay, F., Mallam, S., & Geissler, E. (1992). Scattering properties of polymer gels at the theta temperatur. *Macromolecules*, *25*, 6915–6920.

Hecht, A. M., Horkay, F., & Geissler, E. (2001). Neutron scattering investigations on bimodal polymer gels. *Journal of Physical Chemistry*, *105*, 5637–5642.

Hoffmann, I., Heunemann, P., Prévost, S., Schweins, R., Wagner, N. J., & Gradzielski, M. (2011). Self-aggregation of mixtures of oppositely charged polyelectrolytes and surfactants studied by rheology, dynamic light scattering and small-angle neutron scattering. *Langmuir*, *27*, 4386–4396.

Hoogendam, C. W., de Keizer, A., Cohen Stuart, M. A., Bijsterbosch, B. H., Smit, J. A. M., van Dijk, J. A. P. P., et al. (1998). Persistence length of carboxymethyl cellulose as evaluated from size exclusion chromatography and potentiometric titrations. *Macromolecules*, *31*, 6297–6309.

Horkay, F., Hecht, A. M., Zrínyi, M., & Geissler, E. (1996). Effect of cross-links on the structure of polymer gels. *Polymer Gels and Networks*, *4*, 451–465.

Horkay, F., McKenna, G. B., Deschamps, P., & Geissler, E. (2000). Neutron scattering properties of randomly cross-linked polyisoprene gels. *Macromolecules*, *33*, 5215–5220.

Josef, E., & Bianco-Peled, H. (2012). Conformation of a natural polyelectrolyte in semidilute solutions with no added salt. *Soft Matter*, *8*, 9156–9165.

Kästner, U., Hoffmann, H., Dönges, R., & Hilbig, J. (1997). Structure and solution properties of sodium carboxymethyl cellulose. *Colloids and Surfaces A: Physicochemical and Engineering Aspects*, *123*, 307–328.

Kajiwara, K., & Miyamoto, T. (2005). Progress in structural characterization of functional polysaccharides. In S. Dumitriu (Ed.), *Polysaccharides: Structural diversity and functional versatility* (pp. 1–40). New York: Marcel Dekker.

King, K. W., & Smibert, R. M. (1963). Distinctive properties of beta-glucosidases and related enzymes derived from a commercial Aspergillus niger cellulose. *Applied Microbiology*, *11*, 315–319.

Kjøniksen, A., Nilsson, S., Thuresson, K., Lindman, B., & Nyström, B. (2000). Effect of surfactant on dynamic and viscoelastic properties of aqueous solutions of hydrophobically modified ethyl(hydroxyethyl) cellulose, with and without spacer. *Macromolecules*, *33*, 877–886.

Kjøniksen, A., Nyström, L., & Lindman, B. B. (1998). Effects of temperature, surfactant concentration, and salinity of the dynamics of dilute solutions of a nonionic cellulose derivative. *Langmuir*, *14*, 5039–5045.

Kratky, O., & Stabinger, H. (1984). X-ray small-angle camera with block-collimation system an instrument of colloid research. *Colloid and Polymer Science*, *262*, 345–360.

Kulicke, W. M., Kull, A. H., Kull, W., Thielking, H., Engelhart, J., & Pannek, J. B. (1996). Characterization of aqueous carboxymethylcellulose solutions in terms of their molecular structure and its influence on rheological behavior. *Polymer*, *37*, 2723–2731.

Likos, C. N., Schmidt, M., Lwen, H., Ballauff, M., Ptschke, D., & Lindner, P. (2001). Soft interaction between dissolved flexible dendrimers: Theory and experiment. *Macromolecules*, *34*, 2914–2920.

Likos, C. N., Rosenfeldt, S., Dingenouts, N., Ballauff, M., Lindner, P., Werner, N., et al. (2002). Gaussian effective interaction between flexible dendrimers of fourth generation: A theoretical and experimental study. *Chemical Physics*, *117*, 1869–1877.

Matsumoto, T., & Zenkoh, H. (1992). A new molecular model for complexation between carboxymethylcellulose and alkaline—Earth metal ions in aqueous systems. *Food Hydrocolloids*, *6*, 379–386.

Moan, M., & Wolff, C. (1975). Study of the conformational rigidity of polyelectrolytes by elastic neutron scattering: 1. Carboxymethylcelluloses in the intermediate momentum range. *Polymer*, *16*, 776–780.

Munter, A. (2003). *Scattering length density calculator*. Gaithersburg, MD: National Institute of Standards and Technology, Center for Neutron Research. http://www.ncnr.nist.gov/resources/sldcalc.html (accessed 01.02.12)

Muroga, Y., Yamada, Y., Noda, I., & Nagasawa, M. (1987). Local conformation of polysaccharides in solution investigated by small-angle X-ray scattering. *Macromolecules*, *20*, 3003–3006.

Ngai, K. L., Rajagopal, A. K., & Lodge, T. P. (1990). Star polymer diffusion in concentrated-solutions – Dependence on functionality via the coupling model. *Journal of Polymer Science Part B: Polymer Physics*, *28*, 1367–1377.

Ngai, K. L., Rajagopal, A. K., Rendell, R. W., & Teitler, S. (1986). Models of Kohlrausch relaxations. *IEEE Transactions on Electrical Insulation*, *21*, 313–318.

Ngai, K. L., Rajagopal, A. K., & Teitler, S. (1988). Slowing down of relaxation in a complex system by constraint dynamics. *Journal of Chemical Physics*, *88*, 5086–5094.

Ninan, N., Muthiah, M., Park, I., Elain, A., Thomas, S., & Grohens, Y. (2013). Pectin/carboxymethyl cellulose/microfibrillated cellulose composite scaffolds for tissue engineering. *Carbohydrate Polymers*, *98*, 877–885.

Nyström, B., Kjøniksen, A., & Iversen, C. (1999). Characterization of association phenomena in aqueous systems of chitosan of different hydrophobicity. *Advances in Colloid and Interface Science*, *79*, 81–103.

Orehek, J., Dogsa, I., Tomšič, M., Jamnik, A., Kočar, D., & Stopar, D. (2013). Structural investigation of carboxymethyl cellulose biodeterioration by *Bacillus subtilis* subsp. subtilis NCIB 3610. *International Biodeterioration & Biodegradation*, *77*, 10–17.

Orthaber, D., Bergmann, A., & Glatter, O. (2000). SAXS experiments on absolute scale with Kratky systems using water as a secondary standard. *Journal of Appied Crystallography*, *33*, 218–225.

Rajagopal, A. K., Ngai, K. L., & Teitler, S. (1991). Theoretical aspects of coupling model schemes of slow relaxation in complex correlated systems. *Journal of Non-Crystalline Solids*, *131–133*, 282–288.

Roblin, P., Potocki-Véronèse, G., Guieysse, D., Guerin, F., Axelos, M. A. V., Perez, J., et al. (2013). SAXS Conformational tracking of amylose synthesized by amylosucrase. *Biomacromolecules*, *14*, 232–239.

Schäfer, L., & Elsner, K. (2004). Calculation of the persistence length of a flexible polymer chain with short-range self-repulsion. *European Physical Journal E*, *13*, 225–237.

Schulz, L., Burchard, W., & Dönges, R. (1998). Evidence of supramolecular structures of cellulose derivatives in solution. In T. J. Heinze, & W. Glasser (Eds.), *Cellulose derivatives modifications. Characterization, and nanostructures, ACS. Symp. Ser 688* (pp. 218–238). Washington, DC: American Chemical Society.

Schurz, J. (1983). Molekulare Uneinheitlichkeit und Lösungsinhomogenitat als Kerngrössen von Spinnmassen. *Lenzinger Berichte*, *55*, 12–17.

Sharma, J., & Bohidar, H. B. (2000). Gelatin–glutaraldehyde supramolecular structures studied by laser lightscattering. *Eurpean Polymer Journal*, *36*, 1409–1418.

Shakun, M., Maier, H., Heinze, T., Kilz, P., & Radke, W. (2013). Molar mass characterization of sodium carboxymethyl cellulose by SEC-MALLS. *Carbohydrate Polymers*, *95*, 550–559.

Shakun, M., Heinze, T., & Radke, W. (2013). Determination of the DS distribution of non-degraded sodium carboxymethyl cellulose by gradient chromatography. *Carbohydrate Polymers*, *98*, 943–950.

Turro, N. J. (2005). Supramolecular structure and dynamics special feature: Supramolecular structure and dynamics. *Proceedings of the National Academy of Sciences of the United States of America*, *102*, 10765.

Wandrey, C., Bartowiak, A., & Harding, S. E. (2009). Materials for encapsulation. In N. J. Zuidam, & V. Nedović (Eds.), *Encapsulation Technologies for active food ingredients and food processing* (pp. 31–95). New York: Springer.

Wang, S., Blazek, J., Gilbert, E., & Copeland, L. (2012). New insights on the mechanism of acid degradation of pea starch. *Carbohydrate Polymers*, *87*, 1941–1949.

Yamakawa, H., & Fujii, M. (1974). Intrinsic viscosity of wormlike chains. Determination of the shift factor. *Macromolecules*, *7*, 128–135.

Yuguchi, Y. (2009). Nano-structure analysis of sugar chains by small angle X-ray scattering. *Trends in Glycoscience and Glycotechnology*, *21*, 1–12.

Yuguchi, Y., Urakawa, H., & Kajiwara, K. (2002). The effect of potassium salt on the structural characterization of gellan gum gel. *Food Hydrocolloids*, *16*, 191–195.

Zimm, B. H. (1948). The scattering of light and the radial distribution function of high polymer solutions. *Journal of Chemical Physics*, *16*, 1093–1099.